separations

MDPI

Article

Selective Adsorption of Zirconium Ions from a Mixture of Cations Using Hollow Balls of Oxidized Graphene

Ivan Myroniuk [1], Hanna Vasylyeva [2,*] and Ihor Mykytyn [1]

[1] Department of Chemistry, Vasyl Stefanyk Carpathian National University, Shevchenko St., 57, 76000 Ivano-Frankivsk, Ukraine; myrif555@gmail.com (I.M.); mibius121@gmail.com (I.M.)
[2] Department of Radiation Safety, Uzhhorod University, Narodna Sq. 4, 88000 Uzhhorod, Ukraine
* Correspondence: h.v.vasylyeva@hotmail.com; Tel.: +380-50-977-1740

Abstract

This study investigates the process of selective removal of zirconium cations (Zr^{4+}) from aqueous solutions containing a mixture of cations (Sr^{2+}, Y^{3+}, Zr^{4+}) using hollow balls of oxidized graphene produced by the auto-combustion of saccharide. The physicochemical properties of the synthesized material and the adsorption mechanism were characterized using a range of analytical methods, including SEM/TEM, Raman spectroscopy, FTIR, and X-ray photoelectron spectroscopy (XPS). It has been established that surface oxygen-containing functional groups (-COOH, -OH, epoxy bridges, etc.) play a key role in the adsorption of zirconium. The maximum adsorption capacity for zirconium cations, as measured experimentally, is 232 mg/g. Using inductively coupled plasma mass spectrometry (ICP-MS), it has been demonstrated that in a strongly acidic medium (0.32 M HNO_3, pH = 0–1), the adsorbent exhibits almost 100 percent selectivity in the removal of Zr^{4+} cations from a mixture containing strontium and yttrium, whilst there is no adsorption of Sr^{2+} whatsoever, and the adsorption of Y^{3+} does not exceed 23–25 percent. The results confirm the high efficiency of oxidized graphene in radiochemical separation of the isotopes ^{90}Zr, ^{90}Y, and ^{90}Sr, which is essential for medicine and nuclear forensics.

Keywords: adsorption; separation; zirconium; oxidized graphene; Raman; ICP-MS

1. Introduction

The uncontrolled release of radionuclides into water systems through industrial effluents is a pressing environmental problem, requiring the development of advanced functional materials with enhanced adsorption capacity and environmental safety to effectively capture and immobilize these isotopes. This will help to reduce environmental risks and protect public health. In this context, highly selective adsorption and separation of radionuclides are becoming increasingly important. For example, the separation of rubidium and cesium [1]; cesium and strontium [2]; ^{68}Ge and ^{68}Ga [3]; the selective adsorption of ^{90}Y, ^{90}Sr, and ^{225}Ac ions [4–6]; and the separation of strontium, yttrium, and zirconium have been the subjects of a large number of recent scientific publications [7–9]. On the other hand, the need to extract certain metals, such as zirconium, is driven by technological developments, particularly computer-aided design and manufacturing in the dental sector, which necessitate the efficient recycling of zirconium powder waste. The efficient processing and recycling of zirconium powder are extremely important for recovering valuable metals and reducing environmental impact. The paper [10] examines the process of separating zirconium (Zr^{4+}) and yttrium (Y^{3+}) from waste using the chloride form of the Amberlite

Check for updates

Academic Editor: Dimosthenis Giokas

Received: 30 September 2026
Revised: 5 November 2026
Accepted: 15 November 2026
Published: 23 November 2026

Copyright: © 2026 by the authors. Licensee MDPI, Basel, Switzerland. This article is an open access article distributed under the terms and conditions of the Creative Commons Attribution (CC BY) license.

A27 sorbent. Studies have shown that the adsorbed yttrium is eluted with distilled and deionized water and 1 M HCl, thereby separating it from the zirconium, which remains in the adsorbed state. The separation efficiency of these two elements is 95%.

Zirconium is also used as a cladding material for nuclear reactors. Its purity is crucial to ensuring the reactor's efficiency. The authors of the publication [11] have developed a new composite for the adsorption of zirconium cations. The composite adsorbent was prepared from reduced graphene oxide, grafted with polyacrylic acid, malic acid, and trioctylamine (rGO-g-PAA-MA/TOA) by means of in situ radical polymerization under the action of gamma radiation at a dose of 25 kGy from a ^{60}Co source. The adsorption capacity of the described adsorbent for zirconium ions is 75 mg/g at pH = 0.35. The selective adsorption of zirconium ions from a mixture containing yttrium ions is a pressing issue in medicine, as zirconium-89 is widely used as a contrast agent in positron emission tomography [12–14].

Another scientific task that requires high precision in separating zirconium from isotope mixtures is the age-dating of strontium–yttrium sources in nuclear forensics [8]. To carry out this task, it is important to separate strontium and zirconium—because in the ^{90}Sr-^{90}Y-^{90}Zr chain, yttrium is in secular equilibrium with both the parent isotope strontium and the daughter isotope zirconium. To determine the source's date of manufacture, the ^{90}Zr/^{90}Sr ratio is measured; therefore, it is desirable to separate these two elements as accurately as possible.

Previously (since 1994), hydroxamic acid was proposed for the selective separation of zirconium isotopes from yttrium target atoms [7]. However, at the current stage of research in this field, the range of adsorbents available for separating yttrium and zirconium has expanded considerably [8–11,15,16]. Technologies for the selective adsorption and separation of zirconium isotopes are fairly effective, but they have two drawbacks. The first drawback is that the selective adsorption is not very intensive, so the processes for separating zirconium and associated cations are usually complex and involve multiple stages. The second drawback is that the degree of isotope separation could still be improved [10–13].

Among the adsorbents described for the selective adsorption of zirconium ions, ion-exchange resins, inorganic adsorbents, and their composites play a key role [5–10,13]. On the other hand, oxidized graphene has proven to be an effective adsorbent for a variety of contaminants, including heavy-metal cations [6,14–16].

The aim of this study is to investigate the adsorption of zirconium cations by an adsorbent based on oxidized graphene; to assess the selectivity of this material toward zirconium isotopes and the potential for using oxidized graphene to separate zirconium from strontium and yttrium.

2. Materials and Methods

2.1. Synthesis of the Adsorbent

A well-known method for synthesizing oxidized graphene is the Hummers method [6,15,16]. However, this method requires strong acids and strong oxidizing agents, such as $KMnO_4$. We propose an alternative method for synthesizing oxidized graphene—the self-combustion of saccharides [14,17,18]. The self-combustion of a composite mixture of sucrose, potassium nitrate, and sulfur leads to the formation of a carbonaceous material according to the equation:

$$C_{12}H_{22}O_{11} + 2KNO_3 + S = 9C + 3CO_2 + K_2S + N_2 + 11H_2O \quad (1)$$

For this purpose, beet sugar $C_{12}H_{22}O_{11}$ (DSTU 4623-2006); potassium nitrate KNO_3 (DSTU 1970-74); and ground sulfur, grade 9990 (DSTU 2179-93), were used. Each of these substances was further ground in a ball mill to a particle size of 30 μm. The ratio of the initial reagents was 52% wt. mass of sucrose, 44% wt. mass of potassium nitrate, and

4% wt. mass of sulfur. The flame temperature was 900–1100 °C. The presence of OH^-, CO_3^{2-}, and HCO_3^- anions in the reaction zone leads to the oxidation of individual carbon atoms in graphene and the formation of $\equiv CH_3OH$, -COOH, and –OCOOH groups. Hollow spheres of oxidized graphene form during auto-combustion as a result of the action of pyrolysis gases (water vapor, CO_2). Subsequent carbonization of the bubble shells leads to the formation of hollow carbon balls (Figure 1a–c). The yield of the final product in relation to the starting reagents was 14 percent.

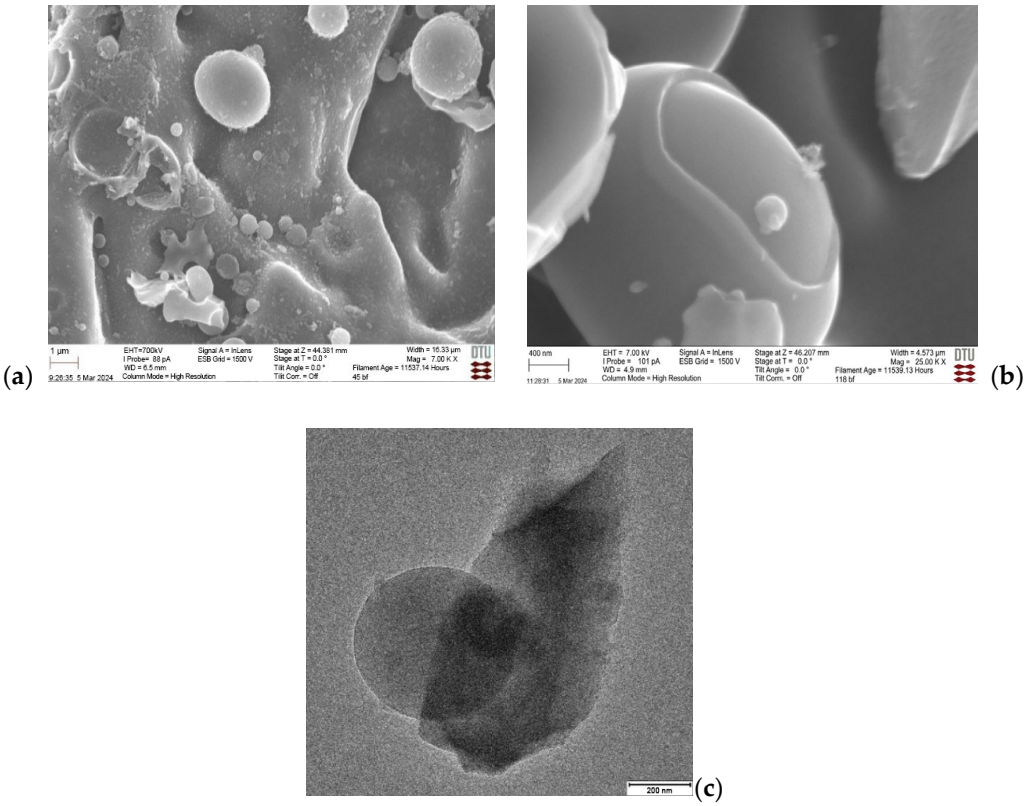

Figure 1. SEM (**a**,**b**) and TEM (**c**) images of hollow balls of oxidized graphene.

2.2. TEM and SEM

The shape and size of the particles were studied using transmission electron microscopy (TEM). A Tecnai T20 G2 microscope (Thermo-Fisher Scientific, Hillsboro, OR, USA) operated at 200 kV was used for image processing. A Zeiss Merlin tabletop scanning electron microscope (SEM) (Carl Zeiss Microscopy GmbH, Oberkochen, Germany), loaded at the Technical University of Denmark (Kongens Lyngby, Denmark) was used to examine the microstructure of the samples under investigation.

2.3. FTIR-Spectroscopy

The IRTracer-100 Fourier transform infrared spectrometer (Shimadzu Corporation, Kyoto, Japan) installed at the 'Laboratory of Experimental and Applied Physics' Center for Shared Use of Scientific Equipment at Uzhhorod University, Uzhhorod, Ukraine, was used for the research.

The spectrometer is equipped with a highly stable He-Ne laser and a thermally stabilized DLATGS detector (Shimadzu Corporation, Kyoto, Japan) for the mid- and far-infrared ranges. The IR spectrometer features LabSolutions IR v2.35 software and a built-in library containing approximately 12,000 spectra across various compound classes.

2.4. Raman Spectroscopy

Raman spectroscopy was carried out using an XploRA™ PLUS spectrometer (HORIBA France SAS, Villeneuve-d'Ascq/Palaiseau, France) with a 532 nm green laser. The laser power was 100 mW. The samples were scanned at power levels of 1 percent and 10 percent, using at least 20 scans (each scan lasting 2 s). The Fityk.1.3.1.exe program and the 'Lorentzian' function were used to analyze the Raman spectra obtained.

2.5. XPS Analysis

The XPS analysis was performed using a Thermo Scientific Escalab 250Xi (Thermo Fisher Scientific, Hillsboro, OR, USA). The analysis was performed in an ultra-high-vacuum environment using an Al Kα (1486.7 eV) X-ray source. The X-ray beam diameter was 650 μm, the transmission energy was 20 eV, and the step size was 0.1 eV. The experiments were performed at a pressure below 10^{-8} Torr and at 294 K. Binding energies were calibrated using a Au foil (the 4f 7/2 binding energy is 83.95 eV). The Casa XPS v2.3.26 rev 1.0 N software was used to analyze the photoelectron results. The Shirley background was used to fit the individual peaks during component analysis.

2.6. Adsorption Investigations

2.6.1. General Methodology for Adsorption Studies

Before investigating the adsorption of zirconium ions from a mixture containing strontium, the general trends in the adsorption of zirconium ions by this adsorbent were studied, namely the dependence of the adsorption amount on the duration of the adsorbate–adsorbent interaction, on the equilibrium concentration, and on the acidity of the solution. To establish general patterns of zirconium cation adsorption, aqueous solutions of zirconium chloride were used. Zirconium chloride is a water-soluble zirconium complex with the formula $[Zr_4\ (OH)_8\ (H_2O)_{16}]\ Cl_8$, more commonly written as $ZrOCl_2{\cdot}8H_2O$.

Adsorption was studied under batch conditions using the single-weighing method. The mass of the adsorbent was typically 0.05 g; the liquid-to-solid phase ratio was 100 (0.05 g of adsorbent–5 mL of the corresponding solution). During the investigation of the dependence of the adsorption value on pH, this ratio was increased to 200 by adding 5 mL of acid or ammonium buffer solution to the reaction mixture to achieve the required pH. Each measurement was repeated three times.

The residual (equilibrium) concentration of the cation under investigation was determined by direct complexometric titration using xylenol orange [19]. Once the duration of the interaction required for the system to reach equilibrium had been determined, experimental studies were conducted to investigate the relationship between the adsorption value and the equilibrium concentration, with a view to plotting the adsorption isotherms.

The adsorption values were calculated using the formula:

$$q_e = \frac{[(C_o - C_e)V]}{m} \quad (2)$$

where q_e—adsorption capacity, mg/g; C_o and C_e—initial and residual (or equilibrium) concentrations of adsorbate, mg/L; V—solution volume, L; and m—mass of adsorbent, g.

The experimental adsorption kinetics were analyzed using four common kinetic models: pseudo-first-order, pseudo-second-order, Elovich, and diffusion (Weber–Morris). The results are presented in the Supplemental File (Tables S1 and S2, Figure S1a–d). The diffusion model provides the most accurate description of the kinetics of zirconium cation adsorption. It can be assumed that the mechanism of zirconium ion adsorption is not chemisorption. Zirconium is most likely adsorbed via two-stage diffusion into the pores of the adsorbent and (in the final stage) via coordination interaction or ion exchange with hydrogen atoms of the functional groups on the surface of oxidized graphene.

Equilibrium adsorption was analyzed using the Langmuir and the Freundlich equations by the non-linear approximation method, using the Excel 'Solver Add-in' software, as recommended by the authors of the publication [20]. In this case, we calculated the R^2 coefficient using the Formula (3):

$$R^2 = 1 - \frac{\sum\left(q_{e,exp}, -q_{e,calc}\right)^2}{\sum\left(q_{e,exp} - q_{e,mean}\right)^2} \quad (3)$$

where $q_{e,exp}$ (mg/g) is the amount of adsorbate adsorbed at equilibrium adsorption; $q_{e,\,cal}$ (mg/g) is the amount of adsorbate calculated using the appropriate equation; $q_{e,\,mean}$ (mg/g) is the arithmetic mean of the experimental adsorption values for a given adsorbate–adsorbent system.

2.6.2. Inductively Coupled Plasma Mass Spectrometry ICP-MS

The concentrations of elements that require separation for medical purposes or nuclear forensics are measured in nanograms per milliliter (ng/mL) [8]. Therefore, to conduct the experiment on the selective adsorption of zirconium cations from a mixture containing strontium and yttrium, we used ultra-pure standards of these cations (see Figure S2 in the Supplemental File). A mixture of strontium, yttrium, and zirconium cations was prepared, containing approximately 10 ng/ml of each element. The experiment was conducted as a one-stage separation process under batch conditions during 60 min of interaction in the 0.32 M HNO_3 medium. The initial and equilibrium concentrations were determined using inductively coupled plasma mass spectrometry. There are five stable isotopes of ^{90}Zr found in nature: ^{90}Zr (51.46%), ^{91}Zr (11.23%), ^{92}Zr (17.11%), ^{94}Zr (17.40%) and ^{96}Zr (2.80%); four stable isotopes of strontium: ^{84}Sr (0.56%), ^{86}Sr (9.86%), ^{87}Sr (7.0%) and ^{88}Sr (82.58%). Yttrium is a mono-isotope: ^{89}Y. Changes in the concentrations of the elements under investigation were assessed by changes in the abundance of specific isotopes: strontium via ^{88}Sr, yttrium via ^{89}Y, and zirconium via the two isotopes ^{90}Zr and ^{91}Zr. Inductively Coupled Plasma Mass Spectrometry (ICP-MS) is an analytical method used to determine trace amounts of elements in a liquid medium. The main advantages of ICP-MS are its high sensitivity for elemental determination and its ability to measure the concentrations of multiple elements simultaneously in a sample [21,22].

The high sensitivity of the ICP-MS method explains its widespread use in nuclear forensics. ICP-MS analysis was carried out on an 'Element-2' mass spectrometer (Thermo Fisher Scientific, Hillsboro, OR, USA). Prior to the analyses, the mass spectrometer was calibrated using 'calibration standard solution A'.

An internal standard of^{103}Rh was also used during the analytical measurements. During a single analytical determination of cation separation, mass spectrometric analysis was carried out on several solutions. Firstly, ICP-MS analysis was carried out on an unseparated mixture of stable strontium, yttrium, and zirconium cations. In this way, the initial concentration of these elements and the efficiency of their detection were monitored, and the possibility of the formation of polyions ^{88}Sr^{16}O, ^{89}Y^{16}O, and ^{90}Zr^{16}O was assessed. To determine the likelihood of ^{89}Y^{1}H polyions forming, a mixture of yttrium and strontium was prepared, but without zirconium. To monitor for potential microimpurities, a 0.32 M HNO_3 solution (blank) was analyzed. ICP-MS analysis of the solution was performed after separation.

3. Results and Discussion

3.1. SEM and TEM Images of Hollow Spheres of Oxidized Graphene

In our previous studies, we showed that this oxidized graphene-based adsorbent is an amorphous material with a well-developed surface. Commonly, these are hollow

balls of oxidized graphene. The total pore volume of the investigated adsorbent is equal to 0.68 $cm^3 \cdot g^{-1}$. The specific surface area is 599.8 $m^2 \cdot g^{-1}$. The volumes of micro- and mesopores are 0.1 $cm^3 \cdot g^{-1}$ and 0.58 $cm^3 \cdot g^{-1}$. The micropores have a size of 0.8–1.0 nm. SEM and TEM images of hollow balls of oxidized graphene are shown in Figure 1a–c.

3.2. Raman Spectroscopy of the Studied Samples

The results of Raman spectroscopy of oxidized graphene spheres before and after the adsorption of zirconium cations from solutions with acidic and neutral pH are shown in Figures 2–5 and Tables 1–3.

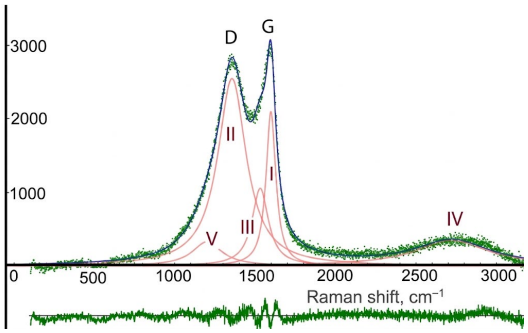

Figure 2. Raman spectrum of oxidized graphene.

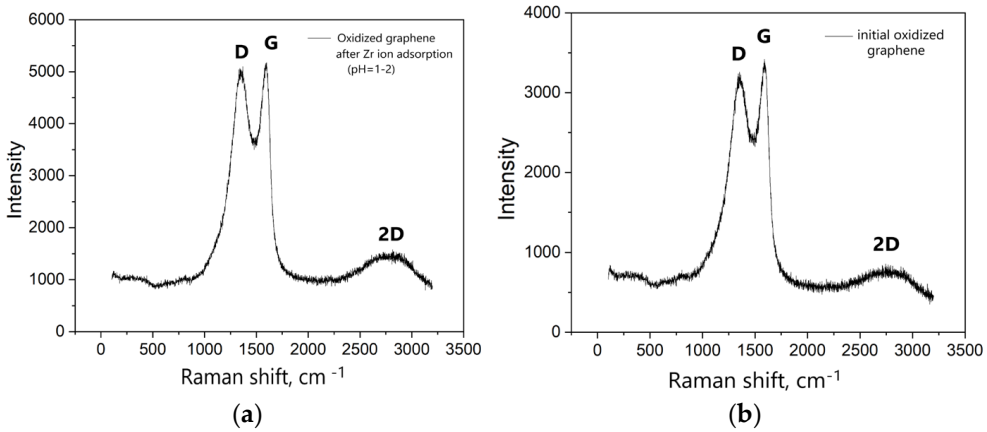

Figure 3. Raman spectra of hollow balls of oxidized graphene: (**a**) before adsorption; (**b**) after adsorption of zirconium cations from an aqueous solution with a pH of 0–1.

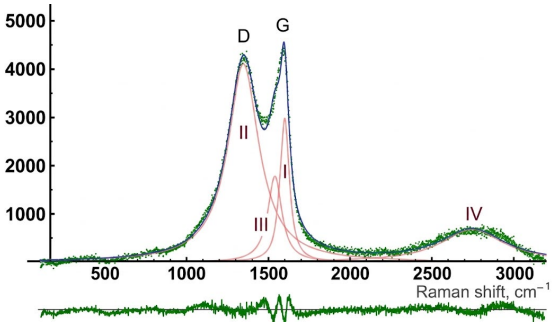

Figure 4. The Raman spectrum of hollow balls of oxidized graphene after adsorption of zirconium ions from an acidic medium, decomposed into its components using the Fityk 1.3.1.exe program.

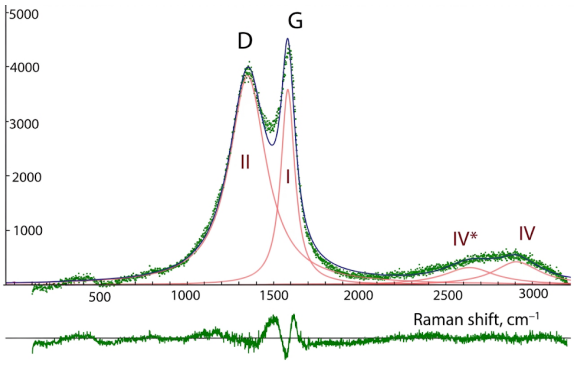

Figure 5. The Raman spectrum of hollow balls of oxidized graphene after adsorption of zirconium ions from an aqueous solution at neutral pH was decomposed into components using Fityk. 1.3.1.exe program and the Lorentzian function. * split peak of graphene clusters.

Table 1. The data of the maxima of the Raman spectrum of oxidized graphene.

Peak	Center	Height	Area	hwhm	Belong to
I	1598	2103.9	242.53	73.389	G
II	1354.97	2244.246	866.28	108.25	D
III	1530.9	1057.98	205.99	61.97	D″
IV	2724.2	343.7	304.55	282	G′ (2D)
V	1199.7	329.48	115.84	111.91	D′

Table 2. The data of the maxima of the Raman spectrum of oxidized graphene after Zr ion adsorption from pH = 0–1.

Peak	Center	Height	Area	hwhm	Belong to
I	1582.5	2103.9	242.54	73.389	G
II	1351.98	4146	143.81	110	D
III	1530.9	1057.98	205.99	61.97	D″
IV	2793.27	696.7	442.49	202	G′ (2D)

Table 3. The data of the maxima of the Raman spectrum of oxidized graphene after adsorption of zirconium ions from an aqueous solution at neutral pH.

Peak	Center	Height	Area	hwhm	Belong to
I	1583.48	3594.9	549.82	48	G
II	1350.44	3839.7	1569.71	130	D
III					D″
IV	2635.5	316	178.45	175.5	G′ (2D)
IV *	2909	421.7	212.14	160	D′

* split peak of graphene clusters.

The G band is associated with the doubly degenerate (iTO and LO) phonon mode (E2g symmetry) at the Brillouin zone center. In fact, the G-band is the only band arising from a normal first-order Raman scattering process in graphene [23].

On the other hand, the band at 2724.2 cm^{-1} is also a G-band originating from a second-order process. Since this G (or G′) band is approximately twice the D band frequency ($\omega G \sim 2\omega D$), some authors prefer to call it the 2D band. However, this two-phonon band is allowed in the second-order Raman spectra of graphene without any kind of disorder or defects.

In the Raman spectra of oxidized graphene, peak V disappears after adsorption of zirconium ions from a solution with an acidic pH. The Raman spectrum of oxidized graphene spheres also loses peak III after adsorption of zirconium cations from a neutral aqueous solution. It is known that these second-order maxima are associated with the vibrations of defects in oxidized graphene. For example, the D″ band comprises one transverse optical phonon and one defect. Consequently, zirconium ions from an aqueous solution (pH = 0–1) are adsorbed in the same way as strontium ions [16] due to surface defects in oxidized graphene.

In a neutral environment, the picture is more complex. Analysis of the Raman spectrum of an adsorbent with zirconium adsorbed on its surface indicates that most defects are involved in the adsorption. This leads to the splitting of the G′ (2D) peak, which, in turn, indicates an increase in the number of layers in oxidized graphene.

It is likely that a layer of adsorbed zirconium complexes is formed. As in the case of strontium cation adsorption onto the surface of hollow balls of oxidized graphene, the zirconium adsorption process had the greatest effect on the second-order peaks III and V, which are associated with the vibrations of sp^2- and sp^3-hybridized carbon atoms and are attributes of surface defects. A more accurate answer about the mechanism of strontium ion adsorption can be obtained from photoelectron spectroscopy results.

3.3. Results of FTIR Analysis

The results of FTIR spectroscopy are shown in Figure 6.

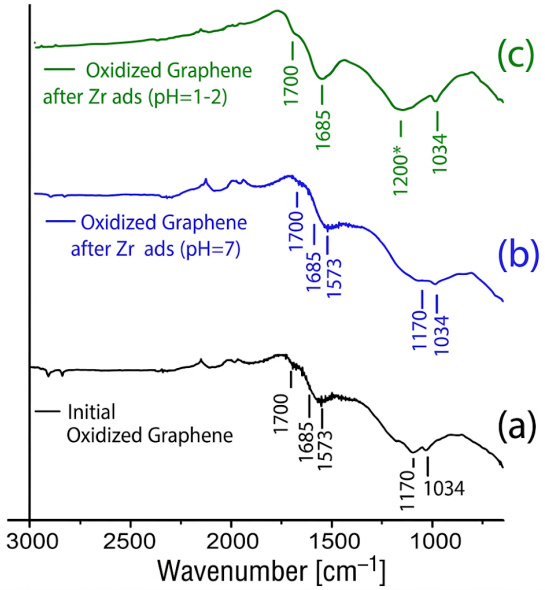

Figure 6. FTIR spectrum of oxidized graphene before and after adsorption: (a) initial oxidized graphene; (b) oxidized graphene after Zr adsorption at pH = 7; (c) oxidized graphene after Zr adsorption in an acidic medium. The asterisk (*) shows that the peak of hydroxyl groups (1170 cm^{-1}) shifted to 1200 cm^{-1} after Zr ion adsorption.

Analysis of the FTIR spectra obtained for hollow balls of oxidized graphene before and after the adsorption of zirconium ions indicates the presence of epoxide groups (vibration at 1034 cm^{-1}) and hydroxyl groups (1170 cm^{-1}). This peak shifts to 1200 cm^{-1} in the oxidized graphene sample after the adsorption of zirconium ions from an acidic medium.

The vibrations of the aromatic double bonds in the graphene lattice are represented in all three spectra by a peak at 1573 cm^{-1}. Water molecules adsorbed onto graphene—or, more precisely, the vibrational oscillations of the surface -OH groups—appear in the spectrum as a band at 1685 cm^{-1}. Consequently, the FTIR results confirm that the graphene is oxidized. The band with maximum absorption at 1700 cm^{-1} corresponds to the C=O bond vibrations in the –COOH groups [24–27].

3.4. Results of XPS Studies

The photoelectron (XPS) spectra of the graphene spheres prior to adsorption are shown in Figure 7a–c and in Table 4.

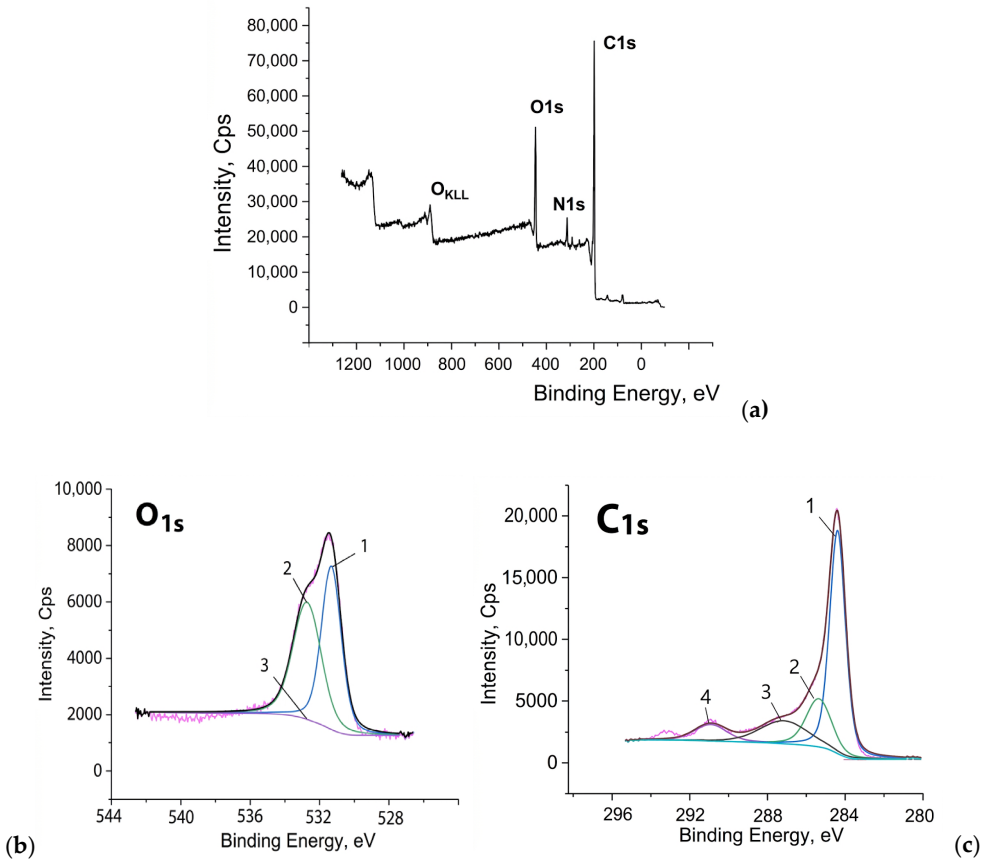

Figure 7. Hollow balls of oxidized graphene before adsorption: (**a**) XPS survey; (**b**) individual oxygen peak; (**c**) individual carbon peak.

Table 4. XPS spectrum of the oxidized graphene (before adsorption).

Figure 7	Maximum Number	Element	FWHM, eV	Relative Area, %	Binding Energy, eV	Groups
(c)	1	C1s	1.223	45.78	284.35	(-C-C)
	2	C1s	1.921	15.55	285.56	(-C=C-)
	3	C1s	4.277	32.00	287.82	(-C-OH)
	4	C1s	2.406	6.67	292.50	(O-C=O)
(b)	1	O1s	1.705	49.74	530.9	(O=C-)
	2	O1s	2.399	50.26	532.64	(-O-C-); -C-OH
	3	-	Shirley background			

The unique phenomenon of zirconium cation adsorption in an acidic environment was confirmed by XPS analysis. The results are shown in Figure 8a–d and the Table 5.

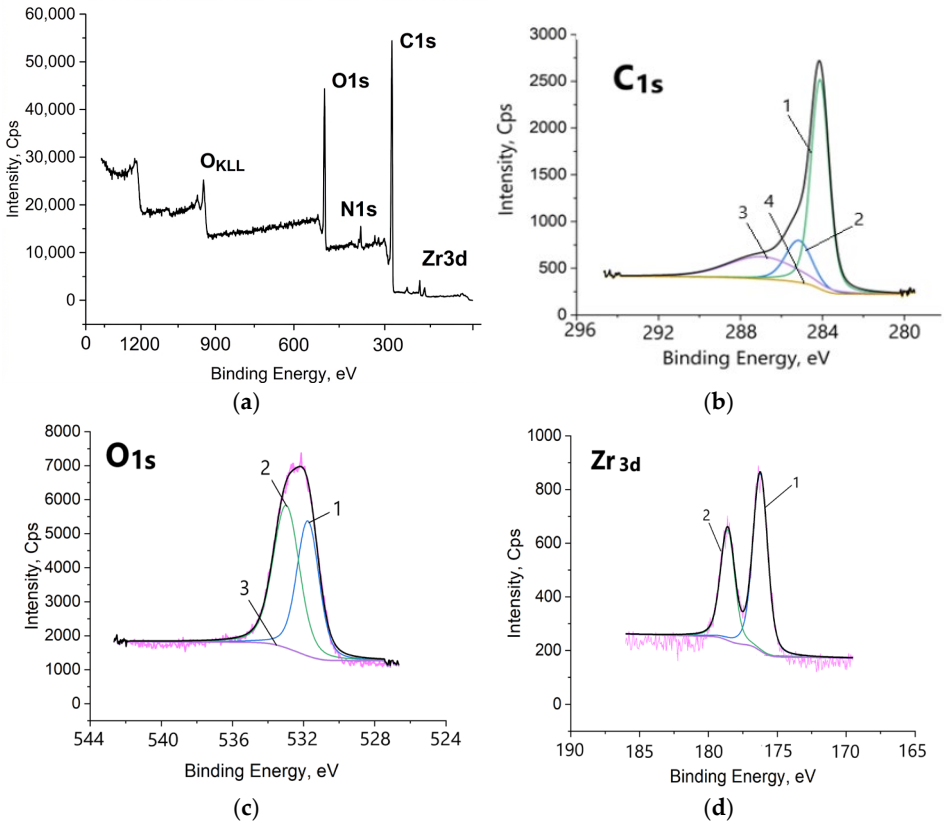

Figure 8. XPS spectrum of oxidized graphene after adsorption of zirconium cations in an aqueous solution at pH = 0–1: (**a**) total XPS spectrum; (**b**) individual carbon peak; (**c**) individual oxygen peak; (**d**) individual zirconium peaks.

Table 5. XPS spectrum of oxidized graphene after adsorption of zirconium cations in an aqueous solution with a pH of 1.

Figure 8.	Maximum Number	Element	FWHM, eV	Relative Area, %	Binding Energy, eV	Groups
(b)	1	C1s	1/1.25	60.65	284.44	(-C-C-) [24–29]
	2	C1s	1.92	19.02	285.56	(-C=C-)
	3	C1s	4.27	20.14	287.82	(-C-OH)
(c)	1	O1s	1/1.84	44.43	531.37	(O=C) (O-C-) (-Zr-O)
	2	O1s	2/2.18	55.57	532.89	(-Zr-OH)
	3	Shirley background				
(d)	2	Zr $3d_{3/2}$	2/1.21	37.71	185.29	ZrO_x
	1	Zr $3d_{5/2}$	1/1.25	62.29	182.91	ZrO_x

The XPS spectra of hollow balls of oxidized graphene after zirconium adsorption from an aqueous solution in a neutral medium are shown in Figure 9a–d and in the Table 6.

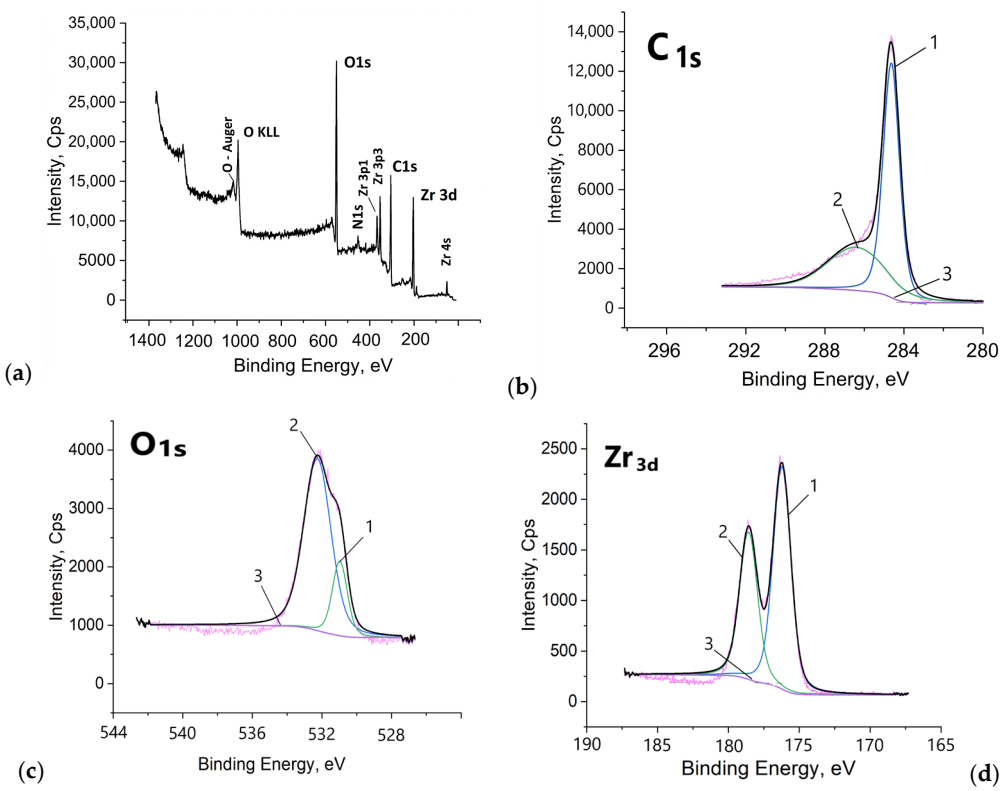

Figure 9. XPS spectrum of oxidized graphene after zirconium cation adsorption from an aqueous solution at pH = 7: (**a**) total XPS spectrum; (**b**) individual carbon peak; (**c**) individual oxygen peak; (**d**) individual zirconium peaks (at pH = 7).

Table 6. XPS spectrum of oxidized graphene after zirconium adsorption at pH = 7.

Figure 9.	Maximum Number	Element	FWHM, eV	Relative Area, %	Binding Energy, eV	Groups
(b)	1	C1s	1.25	61.03	284.79	(-C-C-)
	2	C1s	4.34	38.97	287.00	(H-C-O)
(c)	1	O1s	1.269	19.2	530.39	-C=O, (-Zr-O_2)
	2	O1s	2.31	80.8	532.01	(C-OH) (-Zr-OH)
(d)	2	Zr $3d_{3/2}$	1.49	39.88	185.25	Zr O_x
	1	Zr $3d_{5/2}$	1.49	60.12	182.9	Zr O_x
(a)		Zr 3s			434.78	(Zr-OH_x)
		Zr 3p1			347.78	(Zr-OH)
		Zr 3p3			334.10	(Zr-OH)

The initial ratio of oxygen groups on the surface of the investigated oxidized graphene is as follows: 50.26 percent OH groups and 49.74 percent C=O groups. After the adsorption of zirconium cations from an acidic medium, this ratio shifted to 55.57 percent OH groups and 44.43 percent C=O groups. In other words, adsorption occurs via the surface OH groups of the adsorbent.

Photoelectron spectroscopy of a sample of oxidized graphene with zirconium ions adsorbed onto its surface from a solution with a neutral pH yields particularly interesting results (Figure 9a–d). The ratio of the peaks characterizing surface oxygen-containing groups shifts even further: 80.8% for OH groups and 19.2% for C=O. At the same time, new peaks appear in the energy range 334.10–434.78 eV for the Zr 3s, Zr 3p1, and Zr 3p3

bonds [28–33]. In our opinion, these line data indicate the presence of adsorbed zirconium aquacomplexes on the surface of the adsorbent under investigation.

3.5. Results of Adsorption Studies

The results of the adsorption studies—namely, the kinetic behavior of zirconium ion adsorption, the adsorption isotherm, and the dependence of adsorption on the pH of the solution—are shown in Figures 10a,b and 11, and in Table 7. The adsorption of macroscopic quantities (mg/L level) of zirconium cations by the adsorbent under investigation occurs quite rapidly. Equilibrium is reached within the first 60 min of interaction between the cation solution and the adsorbent surface. Through studies of the equilibrium adsorption of zirconium cations, the maximum adsorption of zirconium ions was experimentally determined to be 232 mg/g. The equilibrium adsorption of zirconium cations (adsorption isotherm) is well described by the Langmuir equation, which may indicate a mechanism of localized adsorption, i.e., adsorption involving adsorption centers.

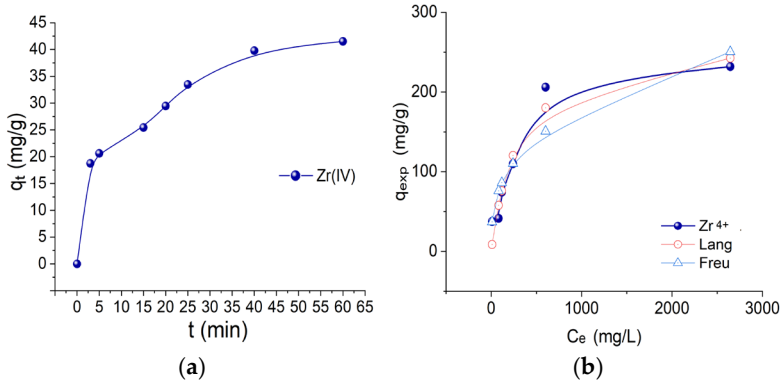

Figure 10. (**a**) Kinetics of Zr (IV) adsorption by oxidized graphene; (**b**) isotherm of Zr ion adsorption by oxidized graphene.

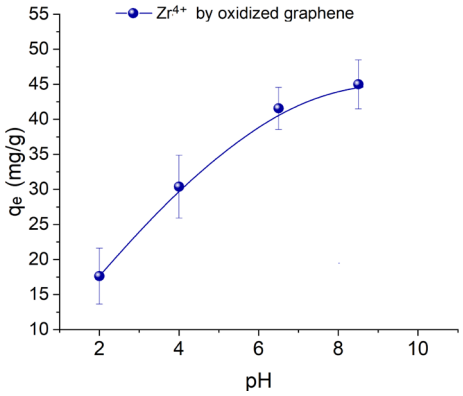

Figure 11. pH dependence of Zr ion adsorption by oxidized graphene.

The dependence of zirconium cation adsorption on solution acidity is shown in Figure 11. The figure indicates that the adsorption values of zirconium cations increase as the pH shifts towards the alkaline region. The chemical properties of zirconium cations play a significant role in this. For example, the zirconium chloride used in this study is a water-soluble zirconium complex with the formula $[Zr_4(OH)_8(H_2O)_{16}]Cl_8$, although it is more commonly denoted as $ZrOCl_2 \cdot 8H_2O$. If we compare the chemical state of zirconium cations in aqueous solutions of different pH values (Table 8) with the corresponding states of yttrium and

strontium, we can see that zirconium tends to form oxyions, hydroxyions, aquacomplexes, and so on.

Table 7. Results of applying the Langmuir and the Freundlich equations to the experimental data on the equilibrium adsorption of zirconium cations by oxidized graphene spheres.

Adsorption Process	Isotherm	Equation	q_e, calc [mg/g]	Parameters	R^2
Zr by oxidized graphene q_e exp = 232 mg/g	Langmuir	$q_e = \frac{q_\infty K C_e}{1 + K C_e}$	242.65	$K_L = 0.00333$ $q_\infty = 270.2$	0.9605
	Freundlich	$q_e = K_f C_e^n$	250.58	$K_f = 16.83$ $n = 0.342$	0.9059

Table 8. Chemical forms of strontium, yttrium, and zirconium cations in aqueous solutions, as functions of pH, according to [34].

Ion/pH	1–3	4–5	6–8	9–11
Sr^{2+}	Sr^{2+}	Sr^{2+}	Sr^{2+}	Sr^{2+}
Y^{3+}	Y^{3+}	Y^{3+}	Y^{3+}, YOH^{2+}	YO^2, HYO aq
Zr^{4+}	Zr^{4+}, ZrO^{2+}	ZrO^{2+}, $ZrOH^{3+}$ $HZrO_2^+$	ZrO^{2+}, $ZrOH^{3+}$ $HZrO_2^+$, $ZrOH_3$	ZrO_2 s $ZrOH_3$, $HZrO_3^-$

In an alkaline environment, zirconium can form insoluble oxides and hydroxides, which precipitate onto the surface. This type of pH-dependent adsorption behavior is characteristic of many cations and adsorbents [5,6,9,14,17,18]. The adsorption of zirconium cations in an acidic environment is half that observed in a neutral or alkaline environment.

However, as demonstrated in [18], the adsorption of strontium ions by this adsorbent in an acidic medium is effectively reduced to zero. Therefore, such conditions are optimal for the separation of trace amounts of strontium, yttrium, and zirconium cations.

3.6. Investigation of Zirconium Separation from the Mixture Using ICP-MS

The results of studies into the selective adsorption of zirconium ions from a mixture containing strontium and yttrium, with the residual concentration of the elements measured using inductively coupled plasma mass spectrometry (ICP-MS), are shown in Figure 12.

The figure illustrates the high selectivity of the graphene-based adsorbent towards trace amounts of Zr^{4+} cations in an acidic medium. Analysis of the concentrations of the isotopes ^{90}Zr and ^{91}Zr shows that, as a result of adsorption, their concentrations fall below background levels. It can be concluded that the concentration of zirconium ions in the solution decreases by two orders of magnitude; in percentage terms, the adsorbent removes 100 percent of the zirconium.

Furthermore, analysis of the plot indicates that the graphene-based adsorbent absorbs a small amount of yttrium from the mixture—approximately 23–25 percent of the initial amount. The amount of ^{88}Sr in the solution increased after adsorption investigations. Simple mathematical calculations suggest that the resulting amount of ^{88}Sr appears to be the sum of the blank contamination and the strontium from the mixture of Sr, Y and Zr. We are as yet unable to explain why the blank contained a comparatively high amount of ^{88}Sr; however, the key point for us is that all the strontium present is in the solution, rather than on the surface of the adsorbent. Zirconium, meanwhile, was completely adsorbed onto the surface of the oxidized graphene (see Table 9).

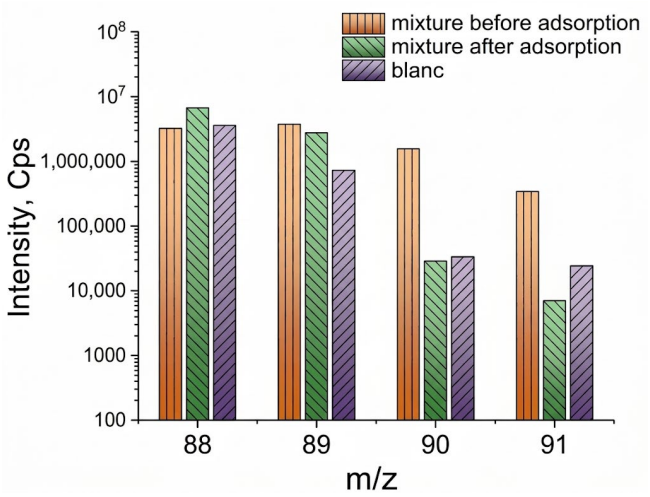

Figure 12. Mass spectrometric studies of a mixture of the isotopes ^{88}Sr, ^{89}Y, and $^{90–91}$Zr before and after interaction with the surface of oxidized graphene.

Table 9. Concentrations of the isotopes under investigation before and after adsorption onto oxidized graphene from a 0.32 M HNO_3 solution.

Isotope	*m*/*z*	Concentration of Isotope [ng·mL^{-1}]/ [Counts per Second, Cps]					
		Before Adsorption	Uncert.	After Adsorption by Oxidized Graphene	Uncert.	Blanc 0.32 M HNO_3	Uncert.
^{88}Sr	88	15.178/ 3,180,768.9	0.113/ 23,771.5	31.93/ 6,693,106.0	0.45/ 94,396.1	16.89/ 3,539,748.8	0.107/ 22,611.1
^{89}Y	89	14.84/ 3,656,361.4	0.077/ 19,069.8	11.115/ 2,737,632.5	0.106/ 26,233.6	2.91/ 718,671.5	0.0358/ 8818.8
^{90}Zr	90	7.34/ 1,539,269.0	0.217/ 45,633.8	0.135/ 28,410.7	0.00084/ 175.8	0.158/ 33,221.4	0.0013/ 276.1
^{91}Zr	91	1.62/ 341,385.5	0.041/ 8631.3	0.0328/ 6885.2	0.000028/ 62.1	0.114/ 23,915.3	0.00125/ 262.8

The question of the mechanism of selective adsorption of zirconium cations in an acidic medium is important, since in an acidic environment (pH = 0–1), the adsorption of zirconium cations occurs under conditions where the adsorbent surface is positively charged and would normally repel positively charged ions, just as happens, for example, with strontium ions. In our view, the high selectivity of the adsorbent towards zirconium cations is due to the large number of oxygen-containing functional groups on the surface of oxidized graphene and the strong complexation ability of zirconium cations.

Although studies of the selective adsorption of zirconium cations were conducted in an environment where the surface of oxidized graphene was predominantly positively charged, the surface still retained functional groups capable of interacting with cations. In other words, even in such an environment, the adsorbent can adsorb a certain number of cations. However, as experimental studies have shown, it did not adsorb strontium cations from the mixture. The adsorption of yttrium cations was also negligible. It is most likely that the surface groups of oxidized graphene act as cation exchangers, and it is well known that, in dilute solutions, cation-exchange resins adsorb higher-charge cations more strongly, for example, as described in [35,36].

The observed selective adsorption of zirconium significantly exceeds the selective adsorption of zirconium by cation-exchange resin, as reported in [35,36]. In our opinion, zir-

conium's ability to form complexes and coordinate with oxygen-containing groups enhances the ion-exchange process and thus ensures highly selective adsorption of zirconium.

4. Conclusions

1. A method involving the auto-combustion of a composite mixture of sucrose, potassium nitrate, and sulfur enables the production of hollow balls of oxidized graphene, highly functionalized with oxygen-containing groups such as -OH, -COOH, epoxide, and carbonyl groups.

2. The Langmuir equation adequately describes the process of equilibrium adsorption of zirconium (R^2 =0.9605), and the experimentally measured maximum adsorption capacity of the material is q_e = 232 mg/g.

3. Analysis of the XPS and FTIR spectra indicates that, in an acidic environment (pH = 0–1), zirconium adsorption occurs predominantly via coordination with surface hydroxyl (-OH) and carbonyl (-C=O) groups, as well as subsequent ion exchange with the proton of the -OH group. At neutral pH, almost all surface defects in the structures are involved in adsorption, accompanied by the formation of zirconium aqua-complexes on the surface.

4. Despite the material's surface having a positive charge at pH = 0–1, the oxidized graphene spheres remove 98 percent of the zirconium cations from the mixture. This is explained by the synergistic effect of cation exchange (due to the higher charge of Zr^{4+} compared with Y^{3+} and Sr^{2+}) and zirconium's high propensity for complex formation.

5. The synthesized adsorbent is a promising material for addressing challenges in nuclear medicine and nuclear forensics (in particular, for the age-dating of the ^{90}Sr-^{90}Y radioactive source), radioecological monitoring, and the disposal of zirconium waste.

Supplementary Materials: The following supporting information can be downloaded at: https://www.mdpi.com/article/10.3390/separations13120349/s1, Figure S1: Applying kinetic models: (a) Elovich, (b) Diffusion model (Weber-Morris), (c) pseudo-second-order, and (d) pseudo-first-order to experimental kinetic adsorption of zirconium cations by hollow balls of oxidized graphene; Figure S2: Ultra-pure standard solutions of strontium, yttrium, and zirconium. Table S1: Kinetic models of adsorption and their linear equations; Table S2: Applying kinetic models: (a) Elovich, (b) Diffusion model (Weber-Morris), (c) pseudo-second-order, and (d) pseudo-first-order to experimental kinetic adsorption of zirconium cations by hollow balls of oxidized graphene.

Author Contributions: Conceptualization, I.M. (Ivan Myroniuk); methodology, I.M. (Ihor Mykytyn); investigation, I.M. (Ivan Myroniuk), H.V. and I.M. (Ihor Mykytyn); writing—original draft: I.M. (Ivan Myroniuk) and H.V. All authors have read and agreed to the published version of the manuscript.

Funding: This research received no external funding.

Data Availability Statement: The original contributions presented in this study are included in the article/Supplementary Material. Further inquiries can be directed to the corresponding author.

Acknowledgments: The authors are greatly thankful to Gean-Claude Grivel (Technical University of Denmark) for supporting the XPS analysis, and Mykola Strilchuk (Nuclear Forensics Laboratory, KINR, Ukraine) for supporting the ICP-MS analysis.

Conflicts of Interest: The authors declare no conflicts of interest.

References

1. Wang, Y.; Fang, D.; Li, K.; Ye, X.; Han, W.; Zhang, P.; Wu, Z.; Shi, G.; Liu, H. Energy window-guided molecular adsorbent for highly selective cesium capture: Breaking the Rb+/Cs+ separation bottleneck. *Chem. Eng. J.* **2026**, *546*, 180340. [CrossRef]
2. Abou-Lilah, R.A.; Elsanafeny, H.A.; Kasem, A.E. Separation of cesium and strontium from real radioactive waste solutions using a high-efficiency cobalt-aluminum silico-tungstate: Batch and column studies. *J. Radioanal. Nucl. Chem.* **2026**, *335*, 6241–6256. [CrossRef]

3. Cressier, D.; Oelsner, S.; Hunter, G.; Quarin, L.; Methot, N.; Wester, D.; Barré, L. Smoothened titania particles to improve radionuclide separation and their application to the development of a novel [^{68}Ge]/[^{68}Ga] generator. *RSC Adv.* **2015**, *5*, 29319–29324. [CrossRef]
4. Huang, D.; Li, Y.; Lei, J.; Feng, X.; Yang, X.; He, R.; Zhang, R.; Wei, H.; Mu, W.; Liu, H.; et al. Engineering surface microenvironment in La-doped Sb_2O_5 for highly efficient separation of strontium from yttrium in strongly acidic media. *Sep. Purif. Technol.* **2026**, *394*, 137568. [CrossRef]
5. Chakraborty, M.; Lee, K.K.; Hasson, A.; Kanagasundaram, T.; Fears, A.; Hu, A.; Wilson, J.J.; Thorek, D.L.J. Stable Chelation of Zr-89 and Ac-225 with Dual Size-Selective Macrocyclic py_2-macrodipa for ^{225}Ac/^{89}Zr Paired Theranostics. *Inorg. Chem.* **2026**, *65*, 16454–16469. [CrossRef] [PubMed]
6. Abd-Elhamid, A.I.; Abu Elgoud, E.M.; Aly, H.F. Sorption behavior of strontium ions by graphene oxide decorated with chitosan nanoparticles from aqueous solutions. *Cellulose* **2024**, *31*, 8203–8220. [CrossRef]
7. O'Hara, M.J.; Murray, N.J.; Carter, J.C.; Kellogg, C.M.; Link, J.M. Tandem column isolation of zirconium-89 from cyclotron bombarded yttrium targets using an automated fluidic platform: Anion exchange to hydroxamate resin columns. *J. Chromatogr. A* **2018**, *1567*, 37–46. [CrossRef] [PubMed]
8. Vasylyeva, H.; Mironyuk, I.; Strilchuk, M.; Mayer, K.; Dallas, L.; Tryshyn, V.; Maliuk, I.; Hryhorenko, M.; Zhukov, O.; Savka, K. Age dating of liquid ^{90}Sr–^{90}Y sources. *Appl. Radiat. Isot.* **2023**, *200*, 110906. [CrossRef] [PubMed]
9. Vasylyeva, H.V.; Mironyuk, I.F.; Mykytyn, I.; Hnylytsia, I.; Vasyliev, A. The influence of the TiO_2 surfaces' chemosorbed fluorine atoms on the adsorption of yttrium and zirconium cations. *Colloids Surf. A Physicochem. Eng. Asp.* **2026**, *728*, 138539. [CrossRef]
10. Abdel Moamen, O.A.; Abu Elgoud, E.M.; Masry, B.A.; Gayed, H.M.; El-Nadi, Y.A.; Borai, E.H. Efficient separation and purification of yttrium from zirconium onto anion exchange sorbent Amberlite A27 from acidic solution. *Appl. Water Sci.* **2025**, *15*, 136. [CrossRef]
11. Ali, A.H.; Abdo, S.M.; Dakroury, G.A.R.S. Zirconium preconcentration from zircon raffinate using gamma radiation–induced polymerization of reduced graphene oxide composite. *Environ. Sci. Pollut. Res.* **2023**, *30*, 58330–58345. [CrossRef] [PubMed]
12. Xu, L.; Xiao, Y.; van Sandwijk, A.; Xu, Q.; Yang, Y. Production of nuclear grade zirconium: A review. *J. Nucl. Mater.* **2015**, *466*, 21–28. [CrossRef]
13. Deri, M.A.; Zeglis, B.M.; Francesconi, L.C.; Lewis, J.S. PET imaging with 89Zr: From radiochemistry to the clinic. *Nucl. Med. Biol.* **2013**, *40*, 3–14. [CrossRef] [PubMed]
14. Mironyuk, I.; Grivel, J.-C.; Vasylyeva, H.; Coşkun, E.; Mykytyn, I.; Mandzyuk, V. Structural-morphological and adsorption properties of hollow balls of oxidized graphene obtained by auto-combustion of saccharose. *Nano-Struct. Nano-Objects* **2025**, *41*, 101462. [CrossRef]
15. Guo, T.; Bulin, C. Adsorption of neodymium (III) over HKUST-1 metal organic frameworks conjugated with graphene oxide: Recovery performance optimization and speciation resolved adsorption mechanism. *Sep. Purif. Technol.* **2026**, *415*, 139796. [CrossRef]
16. Chen, S.; Wu, L.; Wu, Z.; Liu, Z.; Qiu, Z.; Chi, L. Highly efficient removal of Sr^{2+} from aqueous solutions using a polyacrylic acid/crown-ether/graphene oxide hydrogel composite. *RSC Adv.* **2024**, *14*, 7825–7835. [CrossRef] [PubMed]
17. Vasylyeva, H.; Mironyuk, I.; Mykytyn, I.; Strilchuk, M.; Maliuk, I.; Tryshyn, V.; Savka, K. Application of Titanium Dioxide for Zirconium Ions Adsorption and Separation from a Multicomponent Mixture. *Phys. Chem. Solid State* **2021**, *22*, 460–469. [CrossRef]
18. Myroniuk, I.; Vasylyeva, H.; Mykytyn, I.; Grivel, J.-C.; Coşkun, E.; Prokipchuk, I. Highly efficient adsorption of strontium ions from aqueous solutions by hollow balls of oxidized graphene. *Environ. Sci. Pollut. Res.* **2026**, *33*, 10855–10870. [CrossRef] [PubMed]
19. Schwarzenbach, G.; Flaschka, H.A. *Complexometric Titrations*; Irving, H.M.N.H., Translator; Methuen & Co. Ltd.: London, UK, 1969.
20. Tran, H.N.; You, S.-J.; Hosseini-Bandegharaei, A.; Chao, H.-P. Mistakes and inconsistencies regarding adsorption of contaminants from aqueous solutions: A critical review. *Water Res.* **2017**, *120*, 88–116. [CrossRef] [PubMed]
21. Varga, Z.; Nicholl, A.; Mayer, K.; Wallenius, M. Plutonium age dating (production date measurement) by inductively coupled plasma mass spectrometry. *J. Radioanal. Nucl. Chem.* **2015**, *307*, 1919–1926. [CrossRef] [PubMed]
22. Wilschefski, S.; Baxter, M.R. Inductively Coupled Plasma Mass Spectrometry: Introduction to Analytical Aspects. *Biochem. Rev.* **2019**, *40*, 115–133. [CrossRef] [PubMed]
23. Malard, L.M.; Pimenta, M.A.; Dresselhaus, G.; Dresselhaus, M.S. Raman spectroscopy in graphene. *Phys. Rep.* **2009**, *473*, 51–87. [CrossRef]
24. Aliyev, E.; Filiz, V.; Khan, M.M.; Lee, Y.J.; Abetz, C.; Abetz, V. Structural Characterization of Graphene Oxide: Surface Functional Groups and Fractionated Oxidative Debris. *Nanomaterials* **2019**, *9*, 1180. [CrossRef] [PubMed]
25. Tao, W.; Lan, Y.; Zhang, J.; Zhu, L.; Liu, Q.; Yang, Y.; Yang, S.; Tian, G.; Zhang, S. Revealing the Chemical Nature of Functional Groups on Graphene Oxide by Integrating Potentiometric Titration and Ab Initio Calculations. *ACS Omega* **2023**, *8*, 24332–24340. [CrossRef] [PubMed]

26. Korucu, H.; Mohamed, A.I.; Yartaşı, A.; Uğur, M. The detailed Characterization of graphene oxide. *Chem. Pap.* **2023**, *77*, 5787–5806. [CrossRef]
27. Al Kausor, M.; Chakrabortty, D. Analytical techniques for the characterization of graphene oxide. In *Book Comprehensive Analytical Chemistry, Chapter Two*; Kailasa, S.K., Ed.; Elsevier: Amsterdam, The Netherlands, 2024; Volume 106, pp. 39–72. [CrossRef]
28. Briggs, D.; John, T. (Eds.) *Surface Analysis by Auger and X-Ray Photoelectron Spectroscopy*; IM Publications: Chichester, UK; SurfaceSpectra: Manchester, UK, 2003; Available online: https://surfacespectra.com/books/espec/ (accessed on 1 July 2026).
29. Gondal, M.A.; Fasasi, T.A.; Baig, U.; Mekki, A. Effects of Oxidizing Media on the Composition, Morphology, and Optical Properties of Colloidal Zirconium Oxide Nanoparticles Synthesized via Pulsed Laser Ablation in Liquid Technique. *J. Nanosci. Nanotechnol.* **2018**, *18*, 4030–4039. [CrossRef] [PubMed]
30. Kovtun, A.; Jones, D.; Dell'eLce, S.; Treossi, E.; Liscio, A.; Palermo, V. Accurate chemical analysis of oxygenated graphene-based materials using X-ray photoelectron spectroscopy. *Carbon* **2019**, *143*, 268–275. [CrossRef]
31. Tsunekawa, S.; Asami, K.; Ito, S.; Yashima, M.; Sugimoto, T. XPS study of the phase transition in pure zirconium oxide nanocrystallites. *Appl. Surf. Sci.* **2005**, *252*, 1651–1656. [CrossRef]
32. Zirconium Spectra—ZrO_2. Available online: https://xpsdatabase.net/zirconium-spectra-zro2/ (accessed on 1 July 2026).
33. Yao, Y.; Zuo, H.; Liu, Y.; Pang, S.; Lan, L.; Yao, F.; Wu, Y.; Liu, Z. Efficient dye adsorption of mesoporous activated carbon from bamboo parenchyma cells by phosphoric acid activation. *RSC Adv.* **2024**, *14*, 12873. [CrossRef] [PubMed]
34. Atlas of Eh_pH Diagrams: Intercomparison of Thermodynamic Databases. 2005. Available online: https://www.nrc.gov/docs/ML1808/ML18089A638.pdf (accessed on 1 July 2026).
35. Vasylyeva, H.; Mironyuk, I.; Strilchuk, M.; Maliuk, I.; Savka, K.; Vasyliev, O. Adsorption and possibility of separation of heavy metal cations by strong cation exchange resin. *Chem. Phys. Impact* **2021**, *3*, 100056. [CrossRef]
36. Mackay, K.M.; Mackay, R.A.; Henderson, W. *Introduction to Modern Inorganic Chemistry*, 5th ed.; Blackie Academic and Professional: London, UK, 1996; pp. 113–115.

Disclaimer/Publisher's Note: The statements, opinions and data contained in all publications are solely those of the individual author(s) and contributor(s) and not of MDPI and/or the editor(s). MDPI and/or the editor(s) disclaim responsibility for any injury to people or property resulting from any ideas, methods, instructions or products referred to in the content.